SAND2019-14420C

Modeling Pyroshock Attenuation in Cylindrical Space Structures

Daniel Lee* and Vit Babuska †
Sandia National Laboratories, Albuquerque, NM, 87106 USA

Pyroshock events from the actuation of separation devices in satellites and launch vehicles are potentially damaging, very short, high intensity events with high frequency content. The pyroshock damage risk is mitigated somewhat by the fact that the shock intensity is attenuated by the spacecraft structure. The NASA and MIL standards, developed from extensive tests performed in the 1960's, provide pyroshock attenuation guidelines for various structures common to spacecraft and launch vehicles. In this paper, we present the results from a numerical investigation of pyroshock attenuation in cylindrical shell structures. Pyroshock events were modeled using Sandia National Laboratories' engineering mechanics simulation codes, specifically Sierra/SD. Upon verifying the numerical simulation results against a NASA-HDBK-7005 curve, various structural features were added and design variables were varied to investigate their effects on pyroshock wave propagation and attenuation. The results showed that current numerical simulation tools, given appropriate tuning parameters, are capable of modeling pyroshock events in a simple cylindrical geometry at a reasonable cost. The numerical simulations showed that the presence of geometric features had greater attenuating effects than previously understood. However, shock attenuation levels were less sensitive to design variables of the structural features than expected.

Nomenclature

h	=	mesh size (m)
N_t	=	number of time steps (-)
Δt	=	time step (s)
ϵ_{rel}	=	relative error (-)
ζ_{mod}	=	modal damping ratio in Sierra/SD (-)
λ	=	natural frequency (Hz)
λ_{ref}	=	reference natural frequency (Hz)

I. Introduction

Satellites and launch vehicles are subject to pyroshock events that come from the actuation of separation devices. The shocks are very short, high intensity events with high frequency content, that can be damaging events for satellites. The damage risk is mitigated somewhat by the fact that the shock intensity is attenuated by the spacecraft structure. NASA and MIL handbooks and standards provide guidelines for estimating the attenuating effects of distance, joints, and other structural features in the load path between the shock source and the shock sensitive component. Sometimes these rules are not conservative enough, but other times they are grossly over-conservative. Neither situation is good. In the first case, overestimating the attenuation can lead to increased risk of a pyroshock induced failure; in the second case, it can lead to unnecessary and expensive overdesign for a phantom risk.

The guidelines in the NASA and MIL standards were developed from extensive tests performed in the 1960's. This was a long time ago and the origins of the guidelines have largely been forgotten or never passed on to current spacecraft engineers. A better understanding of the bases for the information in the NASA and MIL standards could improve systems engineering and spacecraft designs.

*Graduate Student Intern, Dept. 01557
†Principal Member of the Technical Staff, Dept. 01557, Associate Fellow AIAA

NASA-HDBK-7005 [1] contains the following statement (Section 8.3, pg. 197) in reference to pyroshock effects on small electronic and optical components:

> "With the rapidly increasing capabilities of computer hardware and software, it is possible that finite element method (FEM) models may be developed in the future that can successfully predict these local inputs with sufficient accuracy for design applications."

Today's computational capabilities make it possible to perform virtual pyroshock experiments. The holy grail is a digital twin of a specific satellite or launch vehicle that can provide insight into the effects of pyroshock induced loads. Virtual experiments on a digital twin could provide a more tailored and design specific understanding of pyroshock effects.

This paper describes a project to study a fairly simple pyroshock attenuation problem using computational tools. Specifically, we investigated pyroshock attenuation in a cylindrical structure representative of a rocket body with Sandia National Laboratories' Sierra Structural Dynamics (Sierra/SD) code. Sierra/SD is a massively parallel implementation of structural dynamics finite element analysis, required for high-fidelity, validated models used in modal, vibration, static and shock analysis of weapons systems [2].

We compared our pyroshock attenuation estimates against those in NASA-HDBK-7005 and those obtained by other researchers using a similar approach [3]. We also studied the shock attenuation effects of structural features, specifically bulkheads and electronics boxes, which are common in launch vehicle designs.

Section II provides a brief introduction of the NASA guidelines for pyroshock attenuation and recent numerical studies of pyroshock transmission. Section III describes the details and results of the Sierra/SD numerical simulations. Section IV summarizes the results and findings and draws conclusions about numerically predicting shock attenuation.

II. Pyroshock Attenuation in Cylindrical Structures

Pyroshock is one of the environments to which launch vehicles and spacecraft should be exposed during environmental testing; however, long before a launch vehicle reaches the environmental testing phase, decisions must be made regarding loads on potentially shock sensitive components so they can be designed. This requires an understanding not only of the pyroshock excitation, but also of the loads the shock produces on the component of interest. The pyroshock loads experienced by a component are very dependent on the proximity of the component to the source of the shock. Because of the short duration and high frequency nature of a pyroshock, it will be attenuated by the structural features in the load path between the pyroshock source and the component. The attenuation effects have been handled empirically with guidelines or rules in NASA handbooks [1, 4–6].

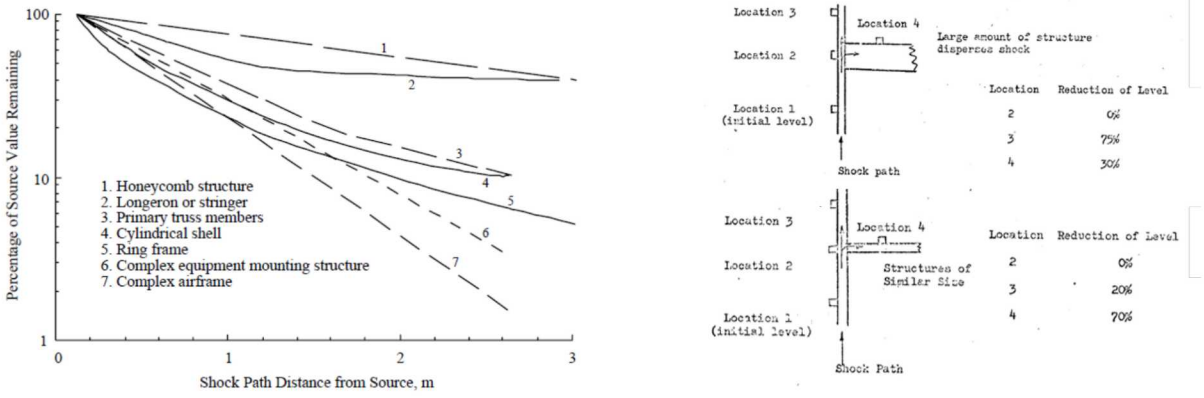

(a) Pyroshock attenuation as a function of distance for various types of structures [1]

(b) Reduction of shock intensity in cylindrical structures due to structural interface [7]

Fig. 1 Legacy guidelines still in use for pyroshock attenuation

Fig. 1a, taken from NASA-HDBK-7005, shows the attenuation of the peak acceleration as a function of the shock path distance from the shock source. In this project we are interested in curve 4—attenuation in a cylindrical shell. Recent studies by Grosserode and Hardt compared the NASA-HDBK-7005 attenuation curve (curve 4 in Fig. 1a)

numerically with a specific cylindrical body subjected to a radial pyroshock in NASTRAN [3, 8]. They found reasonable agreement and concluded that the NASA attenuation curve was reasonably conservative for their structure. Fig. 1b from Ref [7] shows that more complex structures provide a greater degree of attenuation. It shows that structural features, such as bulkheads, reduce shock levels in shell type structures. The figure shows that thick bulkheads should have a larger effect than thin ones. While this figure is essentially a cartoon, lacking dimensions and specific locations of the points, the attenuation levels shown are often used as design guidelines.

Another contributing factor to the reduction of the peak shock levels, one that is not explicitly stated in Ref. [7], is the direction in which the pyroshock acts. The attenuation levels in Fig. 1b are for a radial pyroshock; a longitudinal shock will have very different characteristics as we show in Section III.B.1.

III. Pyroshock Attenuation Modeling in Sierra/SD

The structure that was modeled is a free-free 1.25 m diameter aluminum cylindrical shell, with a nominal length of 2 m. The skin thickness is 4.75 mm. Modal transient analyses were performed using about 1,000 modes, with natural frequencies approximately up to 2 kHz, on three baseline geometries: 2 m long cylinder with zero, one, and two bulkheads. Electronics boxes, represented by point masses connected to the inner surface regions of the cylinder via massless beam elements (i.e., RBE3), also were added to the no- and one-bulkhead cases to study the shock attenuation effects of random objects in the shock paths. The pyroshock input was modeled as a 0.1 ms haversine radial force applied at the bottom end of the cylinder. Details of the geometries and pyroshock inputs are provided in III.A and III.B.1, respectively.

Our quantity of interest was peak acceleration magnitude. “Measurements” were made at various locations along the length of the cylinder and bulkheads (Fig. 2). The nodal acceleration time history data from each "measurement" set were used to plot peak acceleration magnitude attenuation curves with nodeset-2—0.14 m from the source location—peak acceleration magnitude as the reference. To remove the rigid body modes, the measurements were high pass filtered at 5 Hz. Using the cylindrical shell attenuation curve in Fig. 1a as the baseline for the cylinder with no bulkhead, several pretests were performed first to tune model parameters, such as mesh size and modal damping ratio.

A. Geometries

The structures analyzed were free-free 2 m long aluminum cylinders with a radius of 0.625 m with no, one, and two bulkheads as shown in Fig. 2. The locations of the bulkheads were chosen to roughly match the geometry used in Ref [3]. The locations of the nodesets (Table 1) were chosen to keep the mesh sizes and qualities congruent throughout the geometries. The bulkheads were of 50-mm aluminum honeycomb panels, consisting of a honeycomb core with top and bottom sheets. The top and bottom sheets were 4.75 mm thick aluminum. The layered shell elements in Sierra/SD were used to model this sandwich panel with the in-plane equivalent elastic parameters of the aluminum honeycomb core [9].

Table 1 Cylinder and bulkhead nodeset locations

Nodeset	Distance	Nodeset	Distance
1	0.000	9	1.340
2	0.140	10	1.500
3	0.300	11	1.660
4	0.460	12	1.820
5	0.625	13	2.000
6	0.820	51/71/101	0.208
7	1.000	52/72/102	0.417
8	1.180	53/73/103	0.625

Cylinder and bulkhead nodeset distances (in meters) in terms of the shock travel distance. The cylinder nodeset distances are measured from the bottom of the cylinder; and the bulkhead nodeset distances are measured from the outer bulkhead radius to the center.

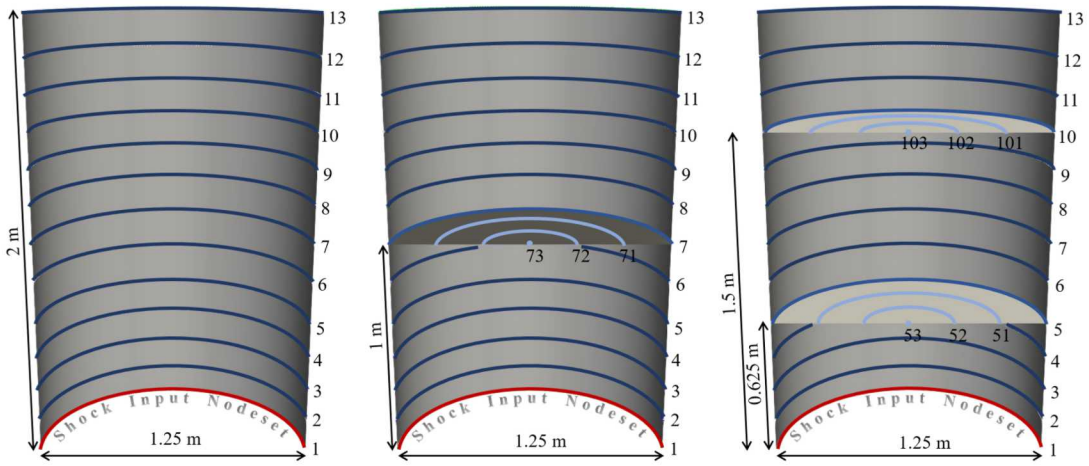

Fig. 2 Cross-sections of no-, one-, and two-bulkhead cylindrical structures analyzed in Sierra/SD. The numbered rings represent the "measurement" locations, referred to as nodesets.

An electronics box was modeled as a point mass connected to a region of the inner surface of the cylinder by massless beam elements. To test the effects of such objects in the paths of a shock, two electronics boxes were added as shown in Fig. 3.

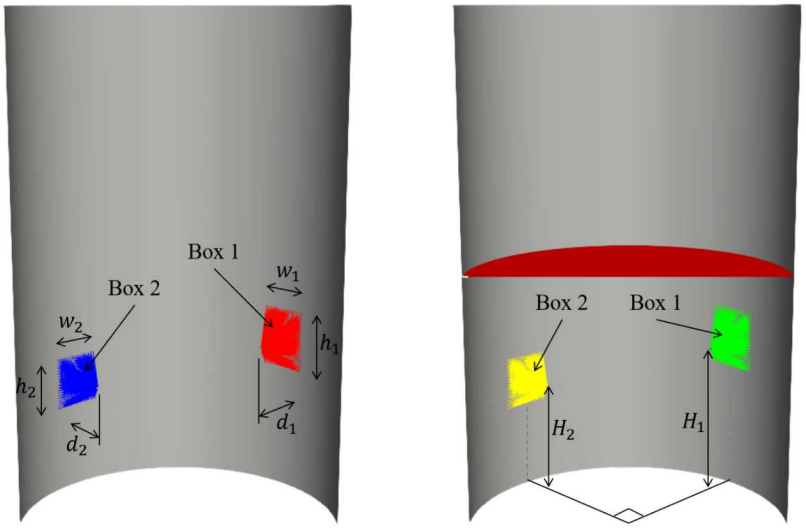

Dimension	Value
h_1	0.196 m
w_1	0.256 m
d_1	0.150 m
H_1	0.625 m
h_2	0.196 m
w_2	0.217 m
d_2	0.150 m
H_2	0.460 m

Fig. 3 No- and one-bulkhead cylinders with electronics boxes represented by point masses

B. Pretests

1. Shock Direction

As mentioned in Section II, the NASA and MIL handbooks and standards do not specify the details of input pyroshock properties associated with the shock attenuation curves. From the numerical simulation point of view, one that affects the simulation results the most, is the direction in which the input pyroshock is applied. Accurate modeling of pyroshock is a complicated task and deserves more attention of its own. Grosserode and Hardt used radial haversine

inputs at the bottom of the cylindrical shell geometries to simulate the pyroshock input [3, 8]. To gain an insight into what kind of shocks best resemble the actual pyroshock, we investigated two types of pyroshock inputs: radial and longitudinal. Both input types were 0.1 ms haversine forces, with magnitude adjusted to amount to a total impulse of 5.4 lbf-s, distributed along the bottom edge of the cylinder.

Fig. 4 shows the differences in initial responses from each shock direction. While the radial shock created a transverse wave, the longitudinal shock created a wave similar to a longitudinal pressure wave along the cylinder skin. The difference between the two shock types was also evident in their attenuation curves (Fig. 5). While the peak acceleration magnitude from the radial shock case was consistent with the NASA attenuation curve, the longitudinal shock was affected by the waves reflected from the open end of the cylinder, resulting in the increase of the peak acceleration magnitude after the midpoint due to constructive interference.

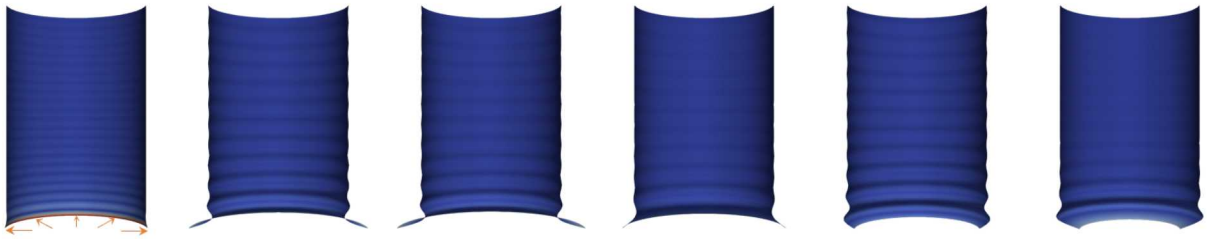

(a) Radial shock

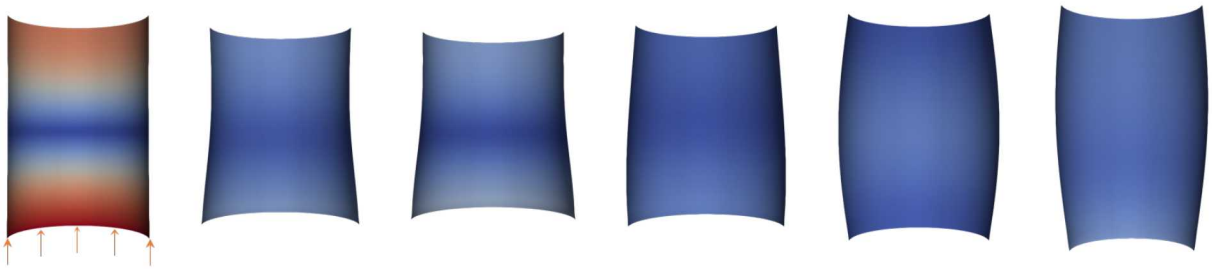

(b) Longitudinal shock

Fig. 4 Initial responses radial and longitudinal shock. Displacements shown here are exaggerated for visual purpose.

2. Mesh Convergence

Four-node quadrilateral shell elements and three-node triangular shell elements were used for the cylinder body and the bulkheads, respectively. Typical mesh refinement tests were done on the no- and one-bulkhead cases to show convergence in natural frequencies. Modal damping ratios ζ_{mod} of 0.02 and 0.03 were used for no- and one-bulkhead cases, respectively. (Details of modal damping study are discussed in III.B.3.) Corresponding pyroshock attenuation curves are plotted as well. Starting with the element size h of approximately 0.05 m, we repeatedly reduced the mesh size by the factor of 1/2 to test element sizes of 0.025 m, 0.0125 m, and 0.00625 m. Natural frequencies from the modal analyses were compared at each refinement level and relative errors were computed as $\epsilon_{rel} = |\lambda_{ref} - \lambda|/\lambda_{ref}$, where λ_{ref} are the natural frequencies from the finest mesh (h = 0.00625 m). As expected, the natural frequencies in the lower modes were very accurate in general, even in the coarsest mesh; while the accuracy decreased with the increasing mode number. The mesh refinement results are plotted in Fig. 6. The mean, minimum, and maximum relative errors at each refinement level are given in Table 2.

3. Modal Damping

Simple global viscous damping models can be applied in Sierra/SD using either modal damping ratios or stiffness and mass proportional damping. To keep the number of tuning parameters low, we applied uniform modal damping in

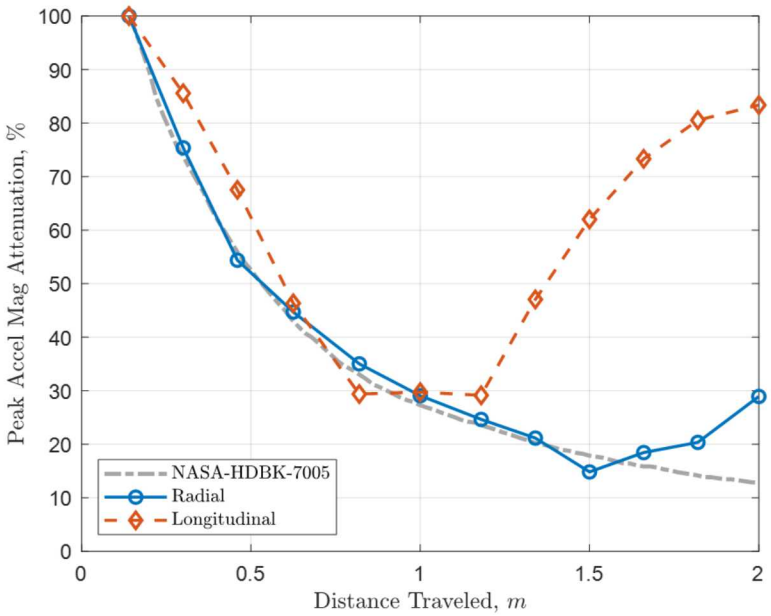

Fig. 5 Radial vs. longitudinal shock attenuation curves

Table 2 Mean, max, and min relative errors

	h	0.05		0.025		0.0125	
		ϵ_{rel}	Mode	ϵ_{rel}	Mode	ϵ_{rel}	Mode
0-bulkhead	Mean	3.2865×10^{-2}		1.1102×10^{-2}		2.3281×10^{-3}	
	Max	5.5780×10^{-2}	800^{th}	2.6620×10^{-2}	901^{st}	5.5783×10^{-3}	940^{th}
	Min	9.8093×10^{-4}	58^{th}	1.3692×10^{-4}	110^{th}	8.7043×10^{-6}	8^{th}
1-bulkhead	Mean	3.1978×10^{-2}		1.0960×10^{-2}		2.3119×10^{-3}	
	Max	6.8682×10^{-2}	912^{th}	2.3347×10^{-2}	899^{th}	5.8805×10^{-3}	934^{th}
	Min	1.8972×10^{-3}	53^{rd}	1.4698×10^{-4}	8^{th}	5.2219×10^{-6}	959^{th}

our models, i.e., a constant modal damping ratio ζ_{mod} was used for the entire frequency range of interest. A parameter study was performed against the NASA attenuation curve to determine the appropriate damping ratios. The mesh size of $h = 0.0125$ m and the radial shock were used for the modal damping tests. Pyroshock attenuation curves (Fig. 7) from the parameter study showed that 2 % ($\zeta_{mod} = 0.02$) modal damping ratio produced the best results. This was the only model parameter that needed to be tuned.

4. Free Boundary Wave Reflection

Figs. 5 and 6e show that our model captured the pyroshock attenuation effect reasonably well relative to the NASA attenuation curve. However, the attenuation behavior diverged from the reference near the end of the cylinder due to the propagated waves reflecting off the free boundary. We investigated these free boundary reflection effects near the ends and explored a way to mitigate it.

The acceleration responses in θ- and z-directions (in cylindrical coordinate) were negligible when a radial shock input was used (Fig. 8a). Time histories of the acceleration magnitudes and the temporal locations of their peak values (Fig. 8) indicated that the propagated waves interfered both constructively and destructively, causing the spikes near the free boundary end of the cylinder.

Using the localized nature of the free-end reflection, we estimated the uncontaminated system response data by moving the free boundary away from the points of interest. In other words, we simply doubled the cylinder height,

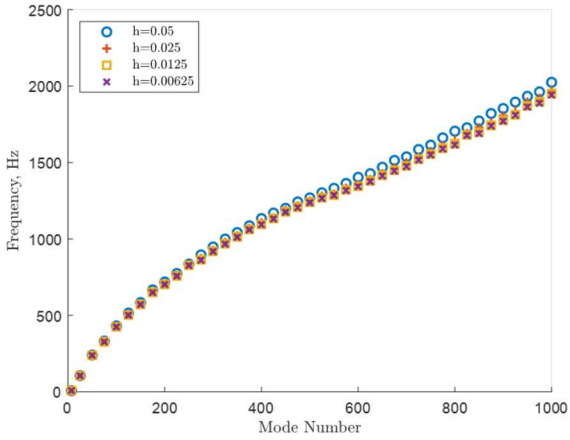

(a) Natural frequencies for the no-bulkhead cylinder

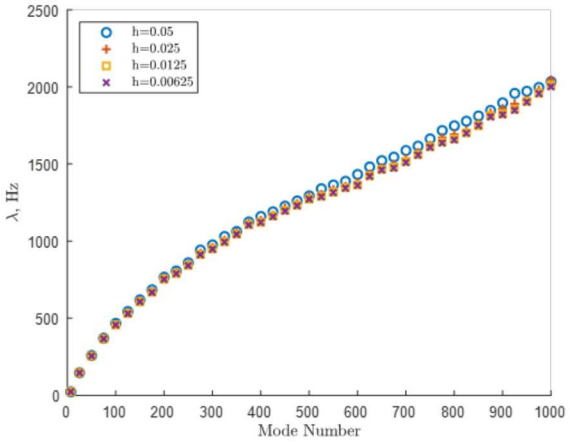

(b) Natural frequencies for the one-bulkhead cylinder

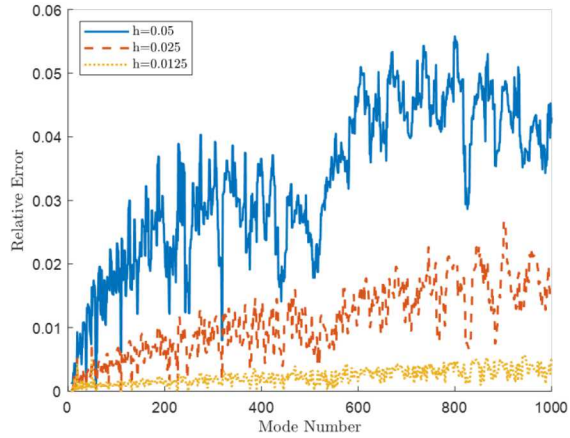

(c) Relative errors of natural frequencies for the no-bulkhead cylinder

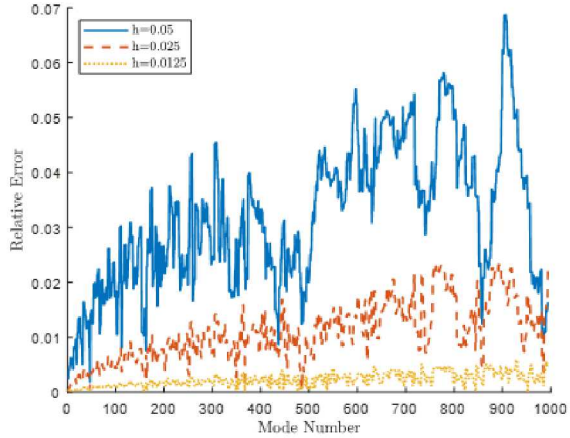

(d) Relative errors of natural frequencies for the one-bulkhead cylinder

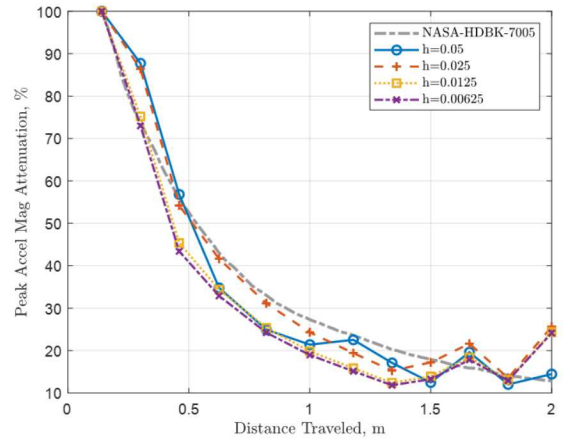

(e) Pyroshock attenuation curve for the no-bulkhead cylinder

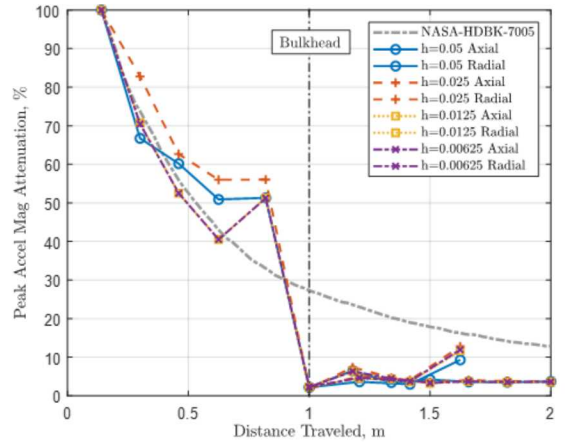

(f) Pyroshock attenuation curve for the one-bulkhead cylinder

Fig. 6 Mesh refinement of no- and one-bulkhead cylinders with $\zeta_{mod} = 0.02$

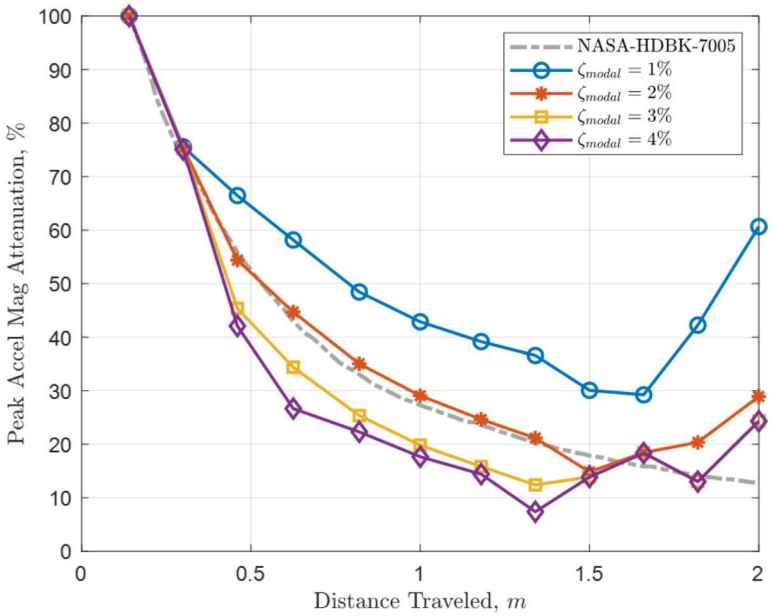

Fig. 7 Pyroshock attenuation curves with various constant modal damping ratios for the no-bulkhead cylinder

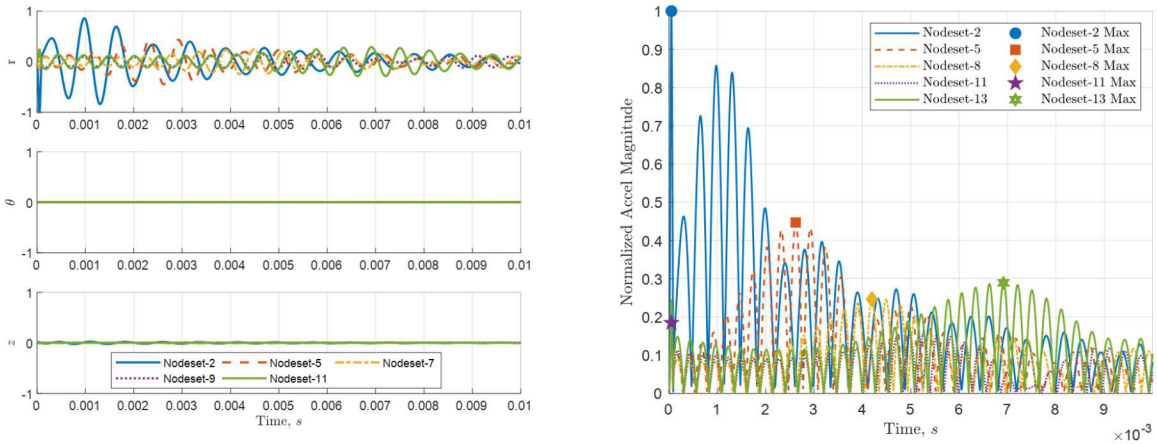

(a) Normalized acceleration **(b) Normalized acceleration magnitude**

Fig. 8 Acceleration and its magnitude time histories

effectively moving the free boundary away from the "measurement" locations. Both radial and longitudinal shock input cases were tested. The results from the lengthened cylinders provided insight into what pyroshock attenuation curves would look like without the free boundary effects (see Fig. 9). The "uncontaminated" pyroshock attenuation curve with radial shock input continued to follow the NASA attenuation curve in the locations (from 1.5 m to 2 m) in which the original simulation curve had diverged. The longitudinal case also benefited from the moved free boundary, confirming that the longitudinal shock input was not representative of a pyroshock event described in the NASA and MIL standards.

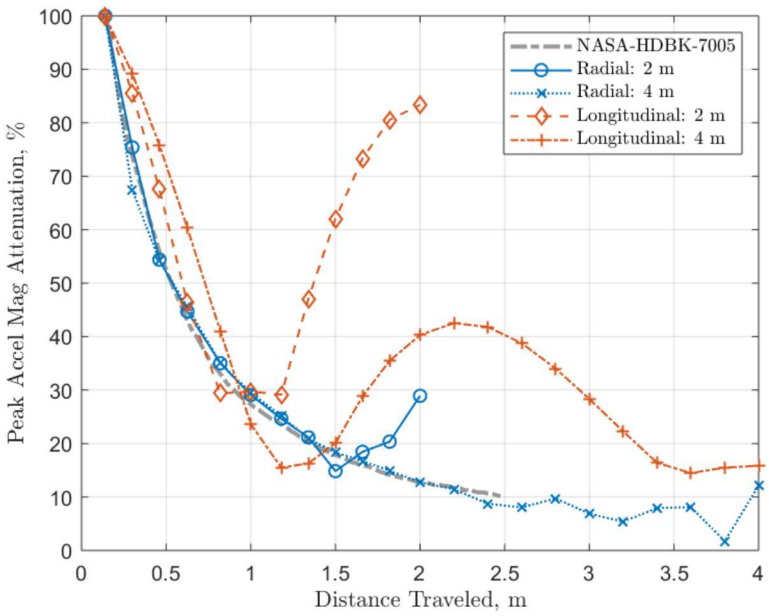

Fig. 9 Pyroshock attenuation curves for 2 m and 4 m no-bulkhead cylinder

5. Pretest Summary and Conclusion

Radial and longitudinal haversine shock inputs were examined. The radial shock produced transverse waves. In contrast, the longitudinal shock gave rise to a wave similar to the pressure waves in the axial direction. Using the NASA attenuation curve as a reference, it was determined that the radial shock input better represented the pyroshock event of interest.

The Sierra/SD modal transient solver was run with 1,000 modes, capturing natural frequencies up to approximately 2 kHz. Convergence of the natural frequencies in the sense of h-refinement was confirmed in the no- and one-bulkhead cylinder models. The convergence test also indicated that the solution converged rather quickly (Figs. 6 and 16), permitting us to use $h = 0.0125\ m$ which saved a significant amount of computational time.

To simplify the tuning process, constant modal damping ratio ζ_{mod} was used for the entire frequency range of interest. The parameter study results showed that the shock attenuation curve could be controlled reasonably well by tuning this one parameter alone. Among various ratio values tested, a 2 % ($\zeta_{mod} = 0.02$) modal damping ratio produced the best result.

Lastly, free boundary wave reflection phenomenon was examined. It was confirmed that polluting effects of the phenomenon could be mitigated by moving the free boundary away from the region of interest (0-2 m). This method proved effective in obtaining "uncontaminated" system responses, but increased the simulation cost—thus, the nominal height of 2 m was used for the actual simulations.

C. Pyroshock Attenuation

With the tuning parameters determined from the pretests (see Table 3), Sierra/SD simulations were performed to obtain pyroshock attenuation curves of the peak acceleration magnitude as a function of the distance traveled and structural features. Simulation details including the number of elements, nodes, and processors used are provided in Appendix V.B. Three specific features were considered: existence of bulkheads, bulkhead thickness, and objects in the shock path.

1. Number of Bulkheads

In Sierra/SD, the bulkheads were modeled with layered shell elements consisting of isotropic top and bottom sheets with an orthotropic honeycomb core section. Note that 50-mm honeycomb panels were considered. Different

Table 3 Sierra/SD simulation settings and tuning parameters

Setting Type	Setting Used	Setting Type	Setting Used
Num of Modes	1,000	Modal Damping Ratio, ζ_{mod}	2 %
Shock Direction	Radial	Time Step, Δt	5e-6 s
Cylinder Height	2 m	Number of Time Steps, N_t	2,000
Mesh Size, h	0.0125 m		

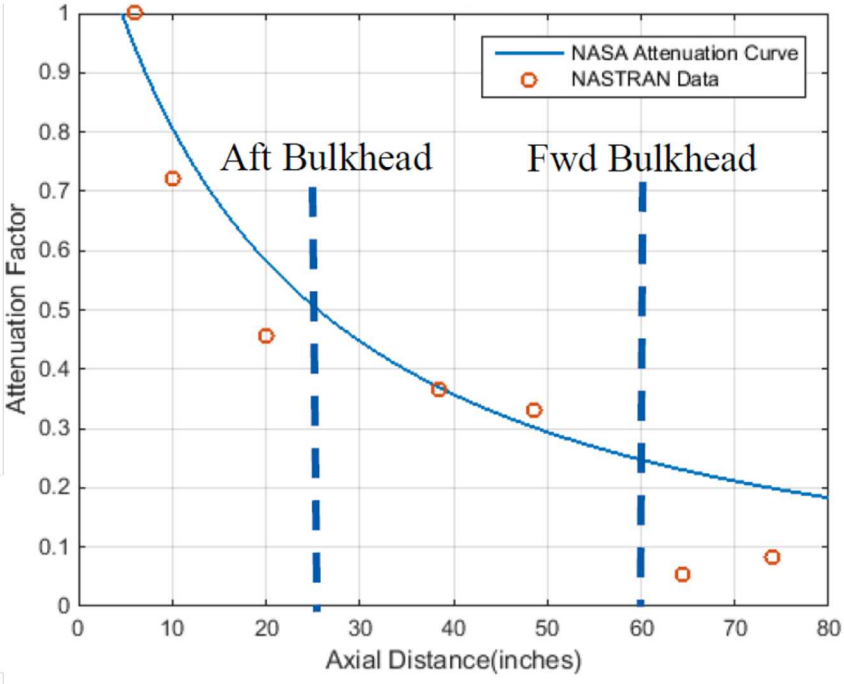

Fig. 10 Attenuation along cylinder skin from Ref [3] using NASTRAN

honeycomb panel thicknesses are discussed in III.C.2.

Pyroshock attenuation curves from the one- and two-bulkhead cases were compared to the no-bulkhead results to assess the effects of bulkheads. In contrast to the results from Ref [3] which used NASTRAN, the peak acceleration magnitude was significantly reduced, down to less than 10 % of the original peak magnitude, by going through just one bulkhead as shown in Figs. 11a and 11b. The attenuation curves of the peak component-wise accelerations, that is, r-, θ-, and z-direction peak accelerations, showed that the bulkheads, effective in reducing the r-direction waves, failed to prevent the propagation of the z-direction waves as illustrated in Figs. 11c and 11d. This was congruent with the results from the longitudinal shock input, which was predominantly in the z-direction. Note that the θ-direction waves in both cases were negligible as expected.

An increase in the peak acceleration magnitude similar to the free boundary wave reflection phenomenon was observed before the skin-bulkhead intersections and at the center of the bulkheads.

2. Bulkhead Thickness

The thickness of the bulkhead in the one-bulkhead case was varied while keeping the simulation settings the same to investigate its impact on pyroshock attenuation. The honeycomb core thickness was varied to consider the following total bulkhead thicknesses: 25, 50, 100, and 200 millimeters. The attenuation curves for the two shock paths, skin-skin and skin-bulkhead, are plotted in Fig. 12. The attenuation did not differ much for the different bulkhead thicknesses in the skin-skin path. The different thickness of the bulkhead did not affect the attenuation levels before the bulkhead. Only the 25 mm thick bulkhead showed different attenuation characteristics before the bulkhead. The attenuation

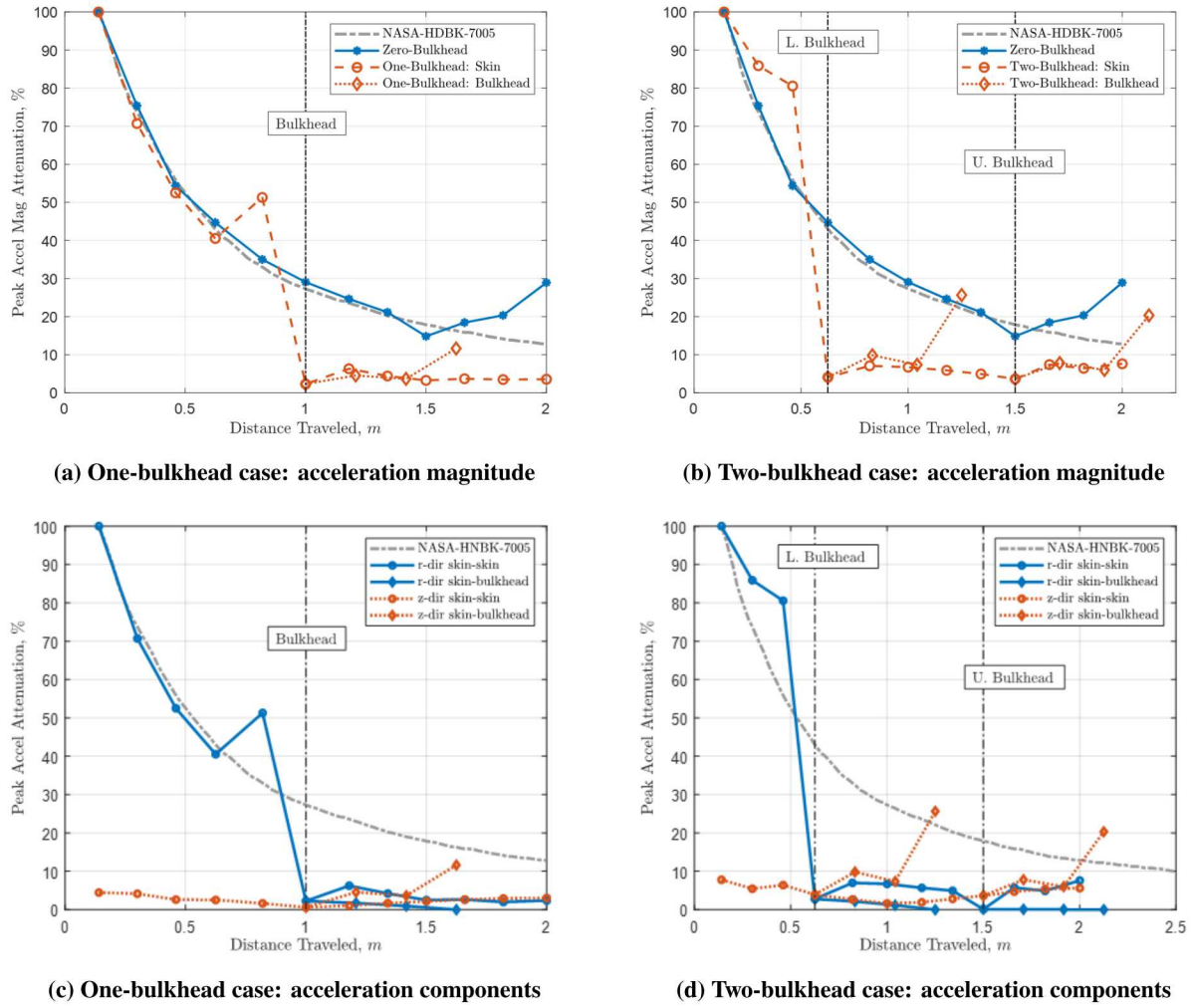

(a) One-bulkhead case: acceleration magnitude

(b) Two-bulkhead case: acceleration magnitude

(c) One-bulkhead case: acceleration components

(d) Two-bulkhead case: acceleration components

Fig. 11 Pyroshock attenuation curves with one- and two-bulkhead cases

levels on the skin aft of the bulkhead were independent of the bulkhead thickness. On the other hand, changing the bulkhead thickness affected the response in the bulkhead, especially at the center. The thinnest, 25 mm, bulkhead showed an increased response at the center because it acted like a thin drum with the r-direction waves transforming into z-direction waves. These results differ from the guidelines shown in Fig. 1b from Ref [7]. Ref. [7] suggests that thicker bulkheads will reduce the response aft of the bulkhead much more than slender bulkheads. We found both slender and thick bulkheads have similar attenuating effects.

3. Shock Path Objects

Ref [3] investigated the level of shock inside an electronics box in a pyroshock event. In our work, we investigated the shock attenuation effect of such a box on the structure to which it is mounted. Two objects, representative of electronics boxes, were added to arbitrary locations on the cylinder in the paths of the shock. The objects were represented by point masses connected to specific nodes in the inner surface of the cylinder by massless beams. The dimensions and the locations of the two electronics boxes are provided in Fig. 3. Based on Ref [10], the density of a typical electronics box was computed and used to assign an appropriate weight to the concentrated masses – 2.5 kg. The attenuation curves from the different paths are plotted in Figs. 14 and 15.

Before the boxes (paths 101 and 103), a spike in peak acceleration magnitude was observed relative to the bare cylinder magnitude as expected (Figs. 14a and 14c). The boxes acted like a bulkhead, greatly reducing the wave intensity

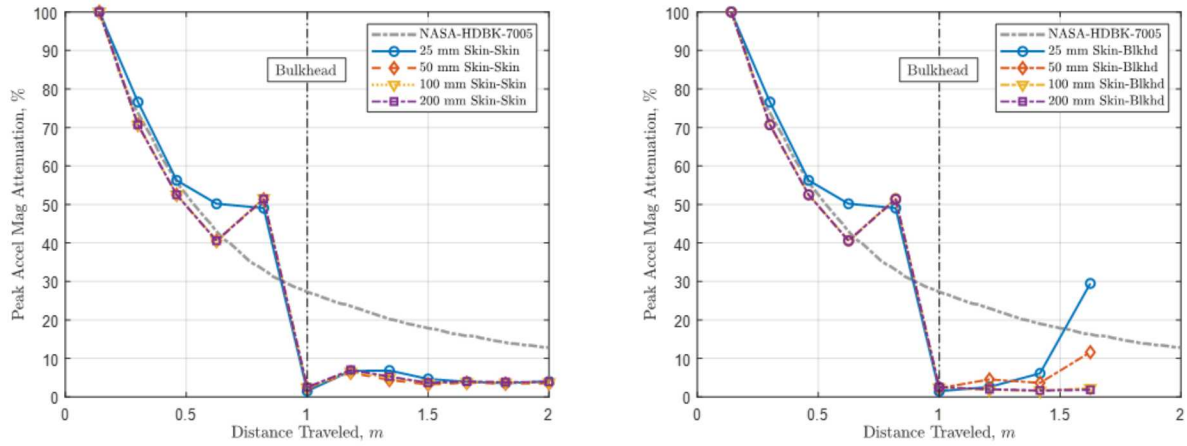

(a) Along the skin-skin path **(b) Along the skin-bulkhead path**

Fig. 12 Pyroshock attenuation curves from various bulkhead thicknesses

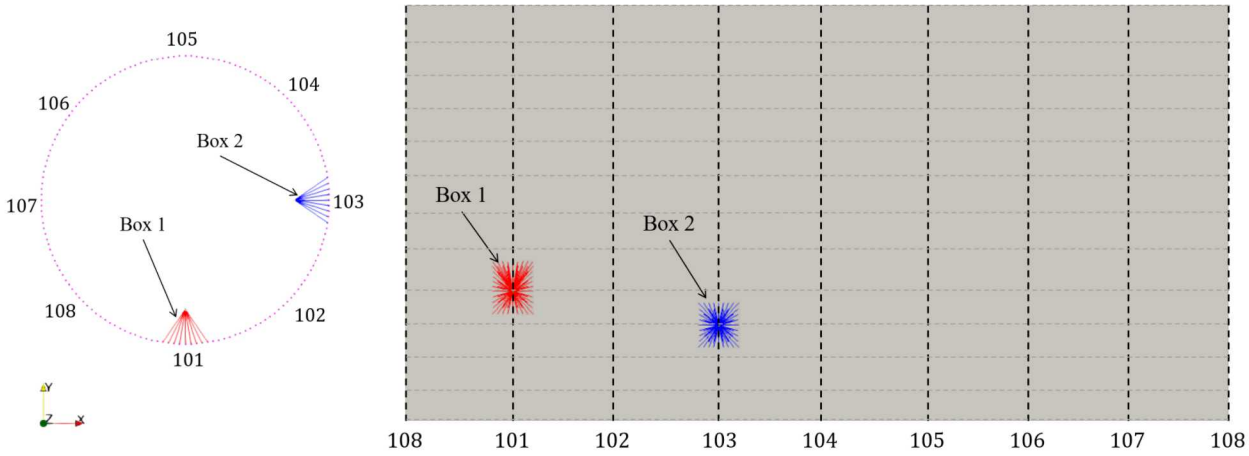

(a) Top view **(b) Expanded cylinder side view**

Fig. 13 Pyroshock paths for the no-bulkhead cylinder with two boxes

immediately aft of them. In contrast to the bulkhead cases, however, constructive interference with unobstructed waves from adjacent paths slightly increased the downstream peak acceleration magnitudes relative to the bare cylinder magnitude. The attenuation curves from the paths without a box (paths 102,104, 105-108) were reasonably consistent with the NASA baseline curve with locally increased responses.

IV. Conclusion

Sandia National Laboratories' massively parallel structural dynamics code, Sierra/SD, was used to numerically study a pyroshock event common in satellite and launch vehicle environments. A cylindrical shell model, representative of a rocket body, was created with quadrilateral and triangle shell elements. Pyroshock events were modeled as radial and longitudinal haversine inputs at the bottom of the cylindrical structure. Three variations of the simple cylindrical model were tested: no-, one-, and two-bulkhead cases. Shock intensity was represented by peak acceleration magnitudes. Several pretests were first performed on the no-bulkhead case against the NASA-HDBK-7005, Fig. 5.8 attenuation curve to determine model tuning parameter values, which were subsequently used in the one- and two-bulkhead cases. For the one-bulkhead case, Sierra/SD results did not match the result from a recent study by Grosserode [3]. The honeycomb sandwich panel bulkhead significantly reduce the intensity of the pyroshock wave to below 10 % of the

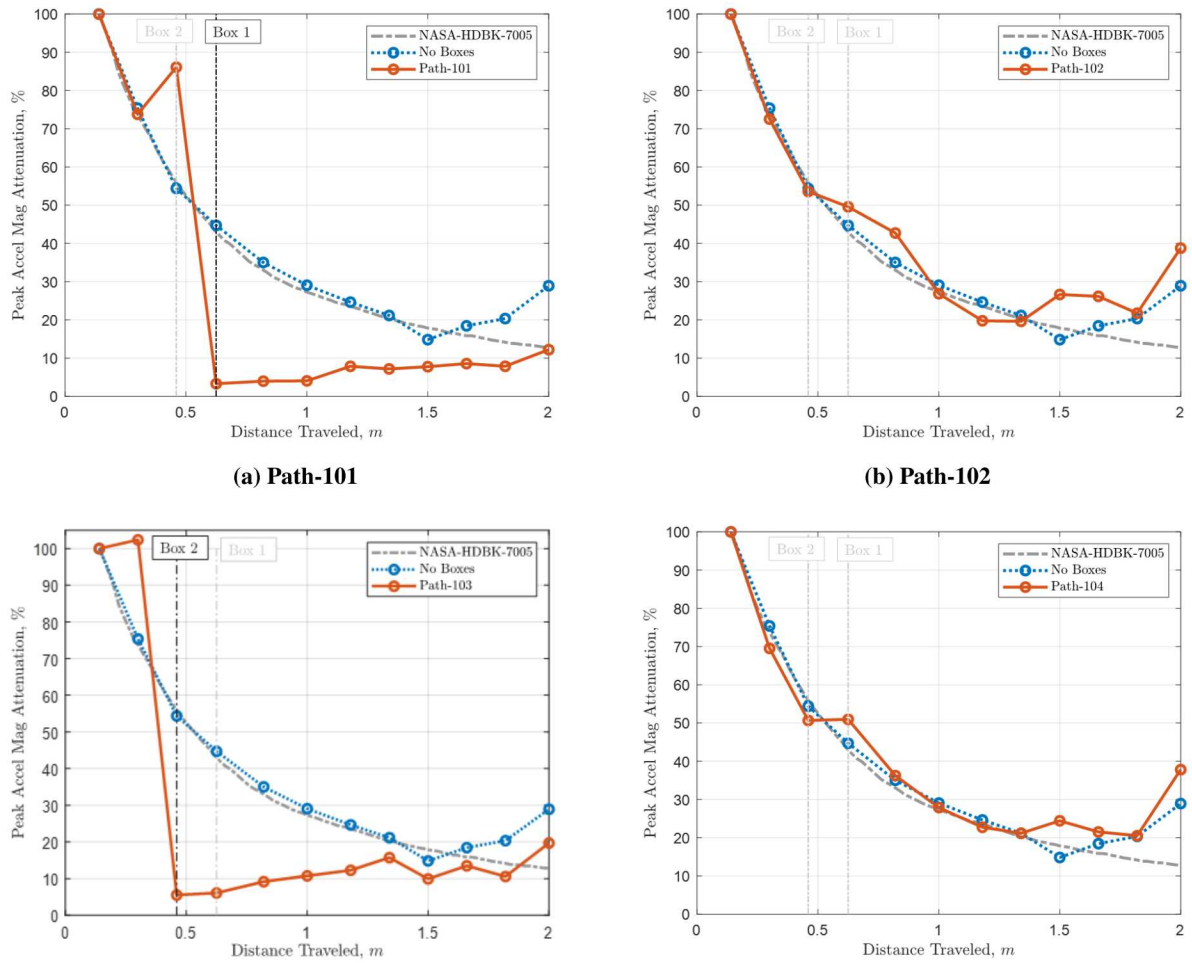

(a) Path-101 **(b) Path-102**

(c) Path-103 **(d) Path-104**

Fig. 14 Pyroshock curves from different shock paths 101-104

reference intensity. In particular, the bulkheads, regardless of the material properties, were exceptionally effective in preventing the r-direction waves. On the other hand, the z-direction wave, a by-product of the radial shock, was amplified as it traveled on the skin-bulkhead path. In contrast to our expectation, the thickness of the bulkhead also had little impact on the attenuating ability on the skin-skin path while adding to the flexural rigidity of the bulkhead. Arbitrary objects, representing electronics boxes, were added to shock travel paths to investigate their impact on wave propagation and shock intensity attenuation. They were found to be a great source of "shock blocker" as they acted like a localized bulkhead. However, breaking the symmetry by adding the boxes caused non-symmetric shock wave patterns and interference, resulting in minor increases in shock intensity downstream, albeit still below the reference curve.

While our work shows that the current numerical tools are sufficiently capable of simulating pyroshock events in simple structures at a reasonable cost, it still remains challenging to determine the tuning parameters required for accurate results. More experimental data from different structures are also needed for further verifying and testing numerical capabilities in modeling shock attenuation.

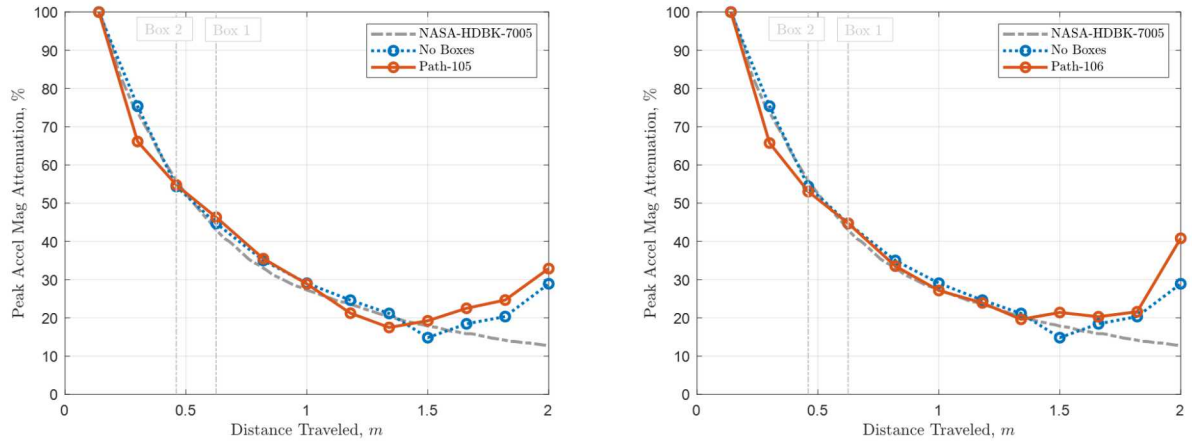

(a) Path-105

(b) Path-106

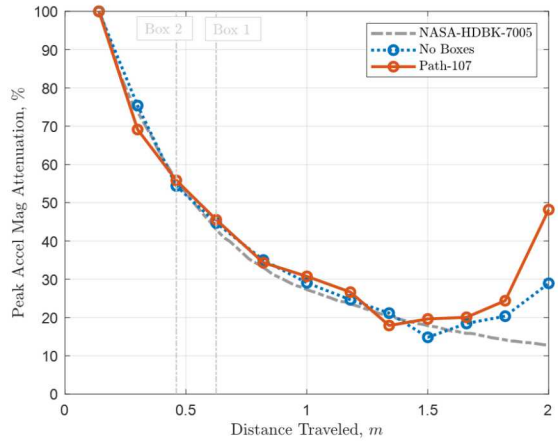

(c) Path-107

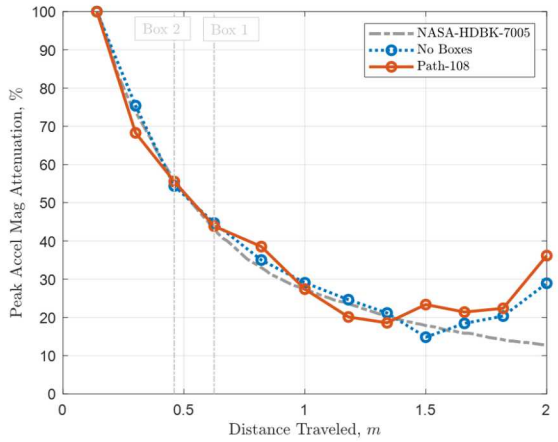

(d) Path-108

Fig. 15 Pyroshock curves from different shock paths 105-108

V. Appendix

A. Sierra/SD Mesh Convergence

Convergence of the mean relative errors in natural frequencies in no- and one-bulkhead cylinder in Sierra/SD are plotted in Fig. 16.

B. Sierra/SD Simulation Settings

The modal transient solver in Sierra/SD is capable of reusing the natural frequencies previously computed, significantly reducing the computation time. In Fig. 4, simulation times marked with an asterisk (*) denote loading in and reusing previously computed data. The cylinder and bulkhead sections were meshed with four-node quadrilateral and three-node triangle elements, respectively. Notice the difference in (wall clock) time for simulations that utilized previously computed data and those that did not.

C. Sierra/SD Input SRS

An SRS of the input radial shock is plotted in Fig. 17.

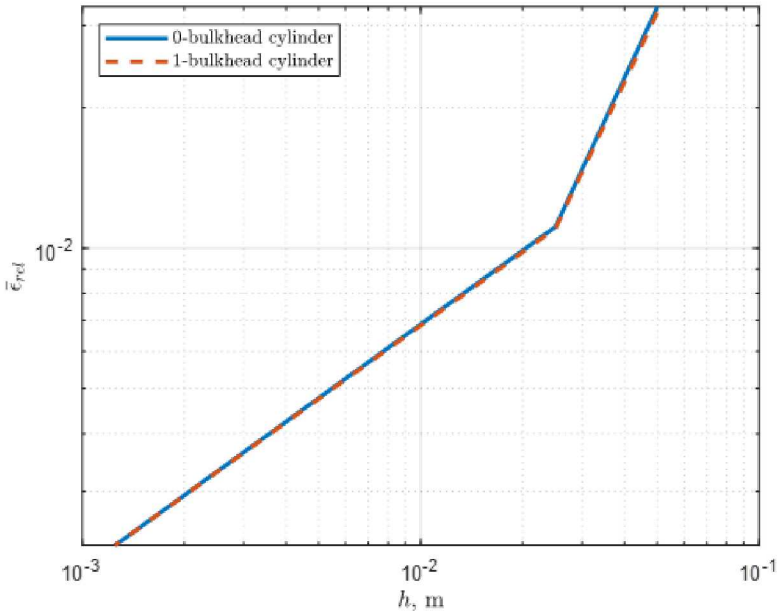

Fig. 16 SD convergence plot for natural frequencies in no- and one-bulkhead cylinder

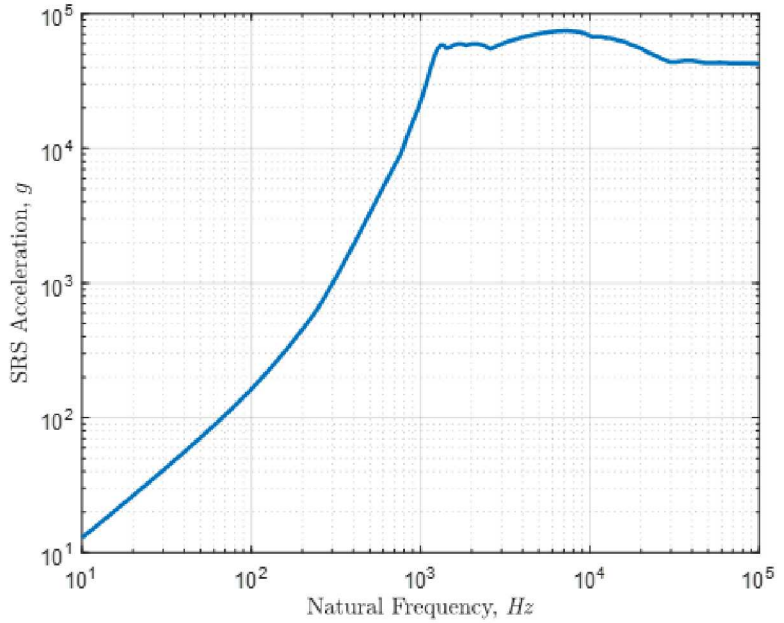

Fig. 17 SRS acceleration of the input

Acknowledgments

Sandia National Laboratories is a multi-mission laboratory managed and operated by National Technology & Engineering Solutions of Sandia, LLC, a wholly owned subsidiary of Honeywell International Inc., for the U.S. Department of Energy's National Nuclear Security Administration under contract DE-NA0003525.

Table 4 Sierra/SD simulation details

Model	h	Elements	Nodes	Processors	Elapsed Time	Δt	N_t
No-Bulkhead	0.05	3,200	3,280	16	0:00:48*	5.00E-06	2000
	0.025	12,480	12,640	16	0:01:08*	5.00E-06	2000
	0.0125	49,920	50,232	20	0:06:39*	5.00E-06	2000
	0.00625	203,504	204,136	20	0:13:39*	5.00E-06	2000
One-Bulkhead	0.05	4,222	3,752	16	0:00:47*	5.00E-06	2000
	0.025	16,656	14,649	32	0:02:10*	5.00E-06	2000
	0.0125	66,920	58,577	32	0:07:47*	5.00E-06	2000
	0.00625	270,746	237,442	40	16:46:01	5.00E-06	2000
Two-Bulkhead	0.05	5,238	4,221	16	0:00:25*	5.00E-06	2000
	0.025	20,846	14,649	16	0:01:43*	5.00E-06	2000
	0.0125	83,968	66,946	32	0:07:56*	5.00E-06	2000
No-Bulkhead	0.05	3,257	3,282	16	0:06:14	5.00E-06	2000
w/ Boxes	0.025	12,502	12,482	16	0:01:07*	5.00E-06	2000
	0.0125	50,619	50,234	20	0:08:45*	5.00E-06	2000
One-Bulkhead	0.05	4,251	3,740	16	0:07:11	5.00E-06	2000
w/ Boxes	0.025	16,530	14,417	16	0:25:21	5.00E-06	2000
	0.0125	83,968	66,946	32	1:44:06	5.00E-06	2000
No-Bulkhead (4 m)	0.0125	99,840	100,152	32	28:10:02	5.00E-06	2000

The first No-Bulkhead simulations are for the 2 m cylindrical structure. h is the mesh size in *meters*; Δt, the time step; N_t, the number of steps. Elapsed time is in *hh:mm:ss* format and the asterisks (*) denote the elapsed simulation times reusing previously computed modal data.

Disclaimer

This paper describes objective technical results and analysis. Any subjective views or opinions that might be expressed in the paper do not necessarily represent the views of the U.S. Department of Energy or the United States Government.

References

[1] Himelblau, H., and et al, "Dynamic Environmental Criteria," , March 2001.

[2] Sierra Structural Dynamics Development Team, "Sierra/SD - User's Notes," , 2019.

[3] Grosserode, P., "A Better Approach to Deriving Shock Environments and Testing," , June 2018.

[4] "Spacecraft Dynamic Environments Testing," , June 2014.

[5] "Pyroshock Test Criteria," , December 2011.

[6] "General Environmental Verification Standard (GEVS) for GSFC Flight Programs and Projects," , April 2013.

[7] Kacena, W., McGrath, M., and Rader, W., "Aerospace Systems Pyrotechnic Shock Data (Ground Test and Flight)," , March 2019.

[8] Hardt, A., "Shock Attenuation vs. Distance for a Cylindrical Shell," , June 2017.

[9] Jiang, D., Zhang, D., Fei, Q., and Wu, S., "An approach on identification of equivalent properties of honeycomb core using experimental modal data," Finite Elements in Analysis and Design, Vol. 90, 2014, pp. 84–92.

[10] Larson, W. J., and Wertz, J. R., "Space mission analysis and design," Tech. rep., Torrance, CA (United States); Microcosm, Inc., 1992.